RSC Advances

PAPER

View Article Online
View Journal | View Issue

Cite this: *RSC Adv.*, 2022, **12**, 3554

Research about the capacitance properties of ion-induced multilayer and self-assembled monolayer $Ti_3C_2T_x$†

Wenwen Ma,[ab] Huaguo Tang,[ac] Tongyang Li,[ad] Lujie Wang,[ad] Lizhi Zhang,[ab] Yuan Yu,[ad] Zhuhui Qiao *[abc] and Weimin Liu[a]

Received 21st October 2021
Accepted 23rd December 2021

DOI: 10.1039/d1ra07771f

rsc.li/rsc-advances

MXenes materials are two-dimensional inorganic materials with abundant surface sites as capacitors. Better control of its morphology and expression of surface groups helps to improve the performance of capacitors. Herein, we controlled the morphology of MXenes with HF, HCl–LiF etching conditions, alkali and metal ions inducing factors. Benefiting from the nanostructures, the capacitance of HCl–LiF-prepared self-assembled monolayer $Ti_3C_2T_x$ soared to 370.96 F g^{-1} from 32.09 F g^{-1} of HF-etched multilaminate $Ti_3C_2T_x$. As a result of the introduction of ions, the surface termination group is replaced by –OH with –F. Profit from this, the alkalized single-deck plicated $Ti_3C_2T_x$ exhibited a supernal capacitance up to 684.53 F g^{-1} because of the wrinkled morphology and more –OH terminal groups. Meanwhile, metal ion abduction brought some negative effects to electrochemical properties due to the oxidation of high-valent metal ions potentially.

1. Introduction

With the advent of graphene, two-dimensional (2D) layered materials have received increasing attention. MXenes, system compounds of two-dimensional metal carbides or nitrides, are insanely competitive in electrochemical energy storage because of their glorious pseudocapacitance properties,[1,2] high metal conductivity,[3,4] and modifiable termination.[5] MXenes (written as $M_{n+1}X_nT_x$, where M is transition metals such as Ti, Cr, V, Zr, Mo, Nb, *etc*; X represents C or/and N; T is F, OH or/and O on behalf of surface groups. $n = 1, 2, 3.$) is synthesized by etching and stripping an "A" layer of MAX (A IIIA or IVA elements, such as Al, Si, Ga, and Ge, usually serve as the "A".) phase with a stratified hexagon crystal structure.[4,6–8]

To date, MXenes have been synthesized predominantly by wet-chemical etching in hydrofluoric acid (HF) or HF-forming etchants such as HCl–LiF.[9–11] It is worth saying that MXenes prepared by HF etching directly are generally multilaminate, whereas those composited by HCl–LiF are few-layer or self-assembled monolayer nanosheets. These MXenes of the two sorts have different layer numbers and surface termination. This leads to different electrochemical properties. For instance, the capacitance of HF-prepared $Ti_3C_2T_x$ only achieves less than 100 F g^{-1}, while those of HCl–LiF-prepared MXenes can achieve 245 F g^{-1}.[4,12] To reveal the differences of the two etching mechanisms profoundly, we researched both the HF etching method and HCl–LiF etching method in detail.

Despite the excellent electrochemical performance of MXene, it is not enough to satisfy us due to the re-accumulation of ultrathin MXene nanosheets during the repeated insertion/extraction process. Therefore it cannot wait to prevent restacking. MXenes are layered inorganic functional materials with a two-dimensional space structure, according to this characteristic, making the molecules of different objects (including organic, inorganic and organic–metal compounds, *etc.*) into the interlayer could keep the layered structure remain the same in the meantime. This idea provides an important way to construct nanocomposites with supramolecular intercalation structures.[4,13–16] An alkali-induced 3D porous network structure is designed to solve the restack problem of layers.[17,18] With the change in the pH of the solution, NaOH induces MXenes to accelerate the flocculation, while abundant –OH with higher chemical reactivity can displace –F as surface groups. Gelation of MXenes induced by metal ions can also maintain an interconnected 3D network.[19] Guided ions can serve as a bridge between nanoscale pieces and destroy the electrostatic repulsive-force between nanosheets, and then the 3D MXene network begins to take shape. As we can see in the paper, divalent metal ions (such as Co^{2+} and Cd^{2+}) have a higher

[a]*State Key Laboratory of Solid Lubrication, Lanzhou Institute of Chemical Physics, Chinese Academy of Sciences, Lanzhou 730000, PR China. E-mail: zhqiao@licp.cas.cn; Tel: +86931-4968193*

[b]*Center of Materials Science and Optoelectronics Engineering, University of Chinese Academy of Sciences, Beijing, 100039, PR China*

[c]*Shandong Laboratory of Yantai Advanced Materials and Green Manufacture, Yantai 264006, PR China*

[d]*Yantai Zhongke Research Institute of Advanced Materials and Green Chemical Engineering, Yantai 264006, PR China*

† Electronic supplementary information (ESI) available. See DOI: 10.1039/d1ra07771f

hydration energy and lower oxidation ability. However, the addition of too many hetero atoms may weaken the electrochemical reactivity, so we will remove the ions up to a point. To reveal the influence of ion induction on the structure and function of MXenes more comprehensively, two induction methods of alkali induction and metal ion induction were introduced.

Herein, we systematically compare of the differences between HF etching multilaminate $Ti_3C_2T_x$ and HCl–LiF etching unilaminar $Ti_3C_2T_x$. To change the surface groups and destroy the interlayer repulsion, MXenes provided by HF portraying or HCl–LiF etching are induced in NaOH liquor or Co^{2+} metal ion solution or Cd^{2+} metal ion solution. Therefore, we can observe the variational electrochemical performance, which is beneficial for the changes in the surface functional groups and the destruction of the interlayer electrostatic repulsion.

2. Materials and experimental procedures

2.1. Synthesis of multilayer MXenes

Multilayer MXenes were prepared by etching Ti_3AlC_2 in hydrofluoric acid (HF) according to reported method.[20] 2 g of Ti_3AlC_2 was slowly added to 20 ml of HF solution and put into an oil bath electromagnetic stirring reaction pot for reaction 24 h at room temperature. The reaction liquid was placed in a 50 ml centrifuge tube and centrifuged 5 times approximately until it was nearly neutral. The ultrasonic separator with a power of 400 W was used for 4 h to remove impurities. Then, the precipitation was centrifuged at 3500 rpm at 20 °C for 60 min. Then, the multilayer MXenes were taken out for freeze-drying.

2.2. Synthesis of monolayer or few-layer MXenes

Such $Ti_3C_2T_x$ was made from Ti_3AlC_2 by reacting in HCl–LiF on the basis of the report.[4,8] 1 g of LiF was accurately weighed and slowly added to 9 M HCl. The solution was mixed in a magnetic agitator for 30 min, and then 2 g of Ti_3AlC_2 was deliberately added while stirring. Put it in a 45 °C oil bath environment and stir for 24 h. Put above liquid in 50 ml of centrifuge tube to wash by deionized water at 5000 rpm in centrifuge approximately 5 times till pH is increased to near neutral. The sediment was desiccated in vacuum and then put in three centrifuger tubes with 30 ml of DI water. The reaction system was stripped in an ultrasonic cleaning machine with a power of 400 W for 4 h. The mixture was placed in a centrifuge at 3500 rpm for 60 min to isolate the supernatant and sediment. Supernatant after separating was what we need. Then, the samples were freeze-dried and redissolved to prepare the MXene single-layer colloid solution at a concentration of 10 mg ml^{-1}.

2.3. Three-dimensional morphology construction of MXenes

Three copies of 3 ml of 10 mg ml^{-1} MXene solutions were removed by direct HF etching and by HCl–LiF preparation method, and then 3 ml of 1 M NaOH solution, 200 μl of 1 M $Co(NO_3)_2$ solution and 200 μl of 1 M $CdCl_2$ solution were dropwise added. The reaction system was reacted for 2 h at room temperature, centrifuged at 8000 rpm at 20 °C for 10 min to remove the remaining doped ions and washed to near neutral in the alkali reaction scheme. Freeze drying to produce MXenes with wrinkles.

2.4. Electrochemical measurements

MXenes powder, acetylene black and PVDF were evenly mixed at a mass ratio of 8 : 1 : 1, coated on copper foil, then vacuum dried at 120 °C for 10 h, and fixed with PET plate, then we made electrode with it. All the electrochemical measurements were conducted in 1 M H_2SO_4 on the electrochemical workstation (CHI 660E, Shanghai) at room temperature with a three-electrode system using Ag/AgCl and platinum electrodes as the reference and counter electrodes, respectively. Particular measurement items and specifications are as follows: the cyclic voltammetry (cyclic voltammetry curve was tested in the potential range −0.55 V to 0 V at a scan rate of 10 mV s^{-1}), EIS (The A.C. Impedance was performed from 10 mHz to 100 kHz from the open circuit potential to the jarless applied voltage), charge–discharge curve (chronopotentiometry was measured at a current density of 1.0 A g^{-1}).

2.5. Materials

Titanium aluminum carbide (200 mesh) was purchased from 11 Technology Co. Ltd. Hydrofluoric acid (HF, ≥40.0%) was purchased from Nanjing Chemical Reagent Co., Ltd. Lithium fluoride (LiF, ≥98.0%), cadmium chloride ($CdCl_2 \cdot 2.5H_2O$, 99.0%), cobalt nitrate hexahydrate ($Co(NO_3)_2 \cdot 6H_2O$, ≥98.5%) and hydrochloric acid (HCl, 36.0–38.0%) were purchased from Sinopharm Chemical Reagent Co. Ltd. Sodium hydroxide (NaOH, ≥96.0%) was purchased from Tianjin Guangcheng Chemical Reagent Co., Ltd.

2.6. Experimental procedures

The three-dimensional morphology of MXene was observed by different methods. The morphology of multilayer and monolayer MXenes induced by different ions was characterized using SEM (JSM-7610F, Japan). The crystal structure of those composites was characterized by XRD (D8 ADVANCE, BRUKER, Germany) using Cu radiation. The surface chemistry of MXenes was measured by XPS (Thermo k-Alpha+) using Al K alpha radiation. The specific surface area (BET surface area) was determined on a Micromeritics ASAP 2460 instrument. All electrochemical tests were conducted on an electrochemical workstation (CHI 660E, Shanghai) at room temperature. Atomic force microscopy (AFM) images were acquired by a Multimode8 (Bruker) AFM system. The macro morphology photo was taken with Huawei p30.

3. Results and discussion

Fig. 1 shows the schematic diagram of preparing all kinds of $Ti_3C_2T_x$ and induced-$Ti_3C_2T_x$ which indicates the synthesis and modification of $Ti_3C_2T_x$. Al layers were selectively etched and removed from the Ti_3AlC_2 precursor by HF and HCl + LiF etching agents due to the weaker M–A bonds than M–X bonds,

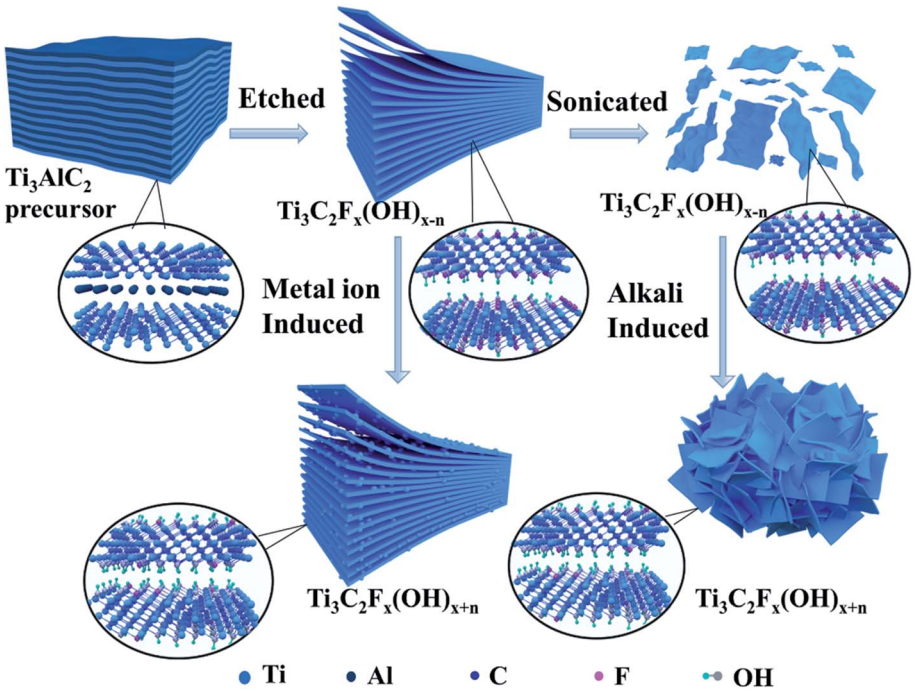

Fig. 1 Mechanism of synthesis and induction of MXenes.

which shows a multilayer morphology similar to accordion. MXene by HCl + LiF prepared can be physically separated 2-D MXenes sheets after the sonication process. Metal ion induction and alkali induction changed the surface groups and morphologies of MXenes in different degrees. Usually, the introduction of metal ions makes the surface terminal group –F replaced by –OH, which destroys the surface electrostatic interaction of MXenes and concurrently increases the layer spacing concurrently. This could help to improve the chemical activity. There are some small protrusions on the surface of HF prepared MXenes, while the HCl + LiF prepared MXenes appeared to be in a folded state because of ion induction.

3.1. Morphological characterization of the samples

As shown in Fig. 2a, the HCl–LiF prepared $Ti_3C_2T_x$ was peeled into a single layer. AFM images of monolayer $Ti_3C_2T_x$ scattered in water show a thickness of approximately 2 nm which proves the single-layer structure (Fig. S1†).[21] However, the multi-layer $Ti_3C_2T_x$ formed by HF etching are accordion-like and connected to a two-dimensional lamellar morphology (Fig. S2a†). The HCl–LiF prepared $Ti_3C_2T_x$ was induced by ions, and the reaction produced flocculation (Fig. 2f). It can be seen that what alkali induced fold states are remarkable (Fig. 2c) greatly expands the surface area of two-dimensional $Ti_3C_2T_x$. Nevertheless, the folds generated by Co^{2+} and Cd^{2+} induction were lower (Fig. 2d and e). However, the various degrees of particles on the multilayer $Ti_3C_2T_x$ surface (Fig. S2†) may affect the layer spacing to some extent. Meanwhile, the change in the XRD (002) peak position could also support this viewpoint.

The low-temperature N_2 adsorption/desorption isotherms (Fig. S3†) and BET surface area (Table 1) prove that ion-induced can inhibit layer restacking. The BET surface area of HCl–$Ti_3C_2T_x$ is only 1.64 $m^2\ g^{-1}$. Which of HCl–OH–$Ti_3C_2T_x$, HCl–Cd–$Ti_3C_2T_x$, HCl–Co–$Ti_3C_2T_x$ is 1.79 $m^2\ g^{-1}$, 6.50 $m^2\ g^{-1}$, 16.43 $m^2\ g^{-1}$. The BET surface area of HF–$Ti_3C_2T_x$ is only 4.61 $m^2\ g^{-1}$. Whom of HF–OH–$Ti_3C_2T_x$, HF–Cd–$Ti_3C_2T_x$, HF–Co–$Ti_3C_2T_x$ is 5.56 $m^2\ g^{-1}$, 6.87 $m^2\ g^{-1}$, 8.27 $m^2\ g^{-1}$. It is noted that metal ions-induced can greatly improve the specific surface area. HCl–LiF prepared $Ti_3C_2T_x$ has a greater potency of restacking because of the monolayer structure, so the changes of this are more distinct than HF prepared $Ti_3C_2T_x$.

3.2. Structural analysis of the samples

The X-ray diffraction patterns (XRD) of HCl–LiF-prepared $Ti_3C_2T_x$ and HF-prepared $Ti_3C_2T_x$ are shown in Fig. 3 The characteristic peak of 10° (002) which represents Ti_3AlC_2 is obviously weakened and shifted to a low angle, while the (104) peak significantly disappears, which means the dislodging of the Al atom layer in Ti_3AlC_2 and the production of $Ti_3C_2T_x$.[4,5] The weakening and disappearance of a series of (001) peaks are caused by the disorder of the nanosheets. HF-etched $Ti_3C_2T_x$ and HCl–LiF-prepared $Ti_3C_2T_x$ have the same ultrasonic stripping process without the ion intercalation. The spectral peak of HF-prepared $Ti_3C_2T_x$ has a smaller variation, which means the different orderliness of the two kinds of MXenes. The obvious spectrum peaks weakened after ion-induced represent the process of ion intercalation. However, it's hard to detect obvious induced ions in the graph, which means that intercalated ions are likely to fall off. The above phenomenon proves that the ions in this experiment only play the role of inducement. No phanerous (104) peak that belongs to MAX is observed in the XRD spectra of the two samples before and after induction, which

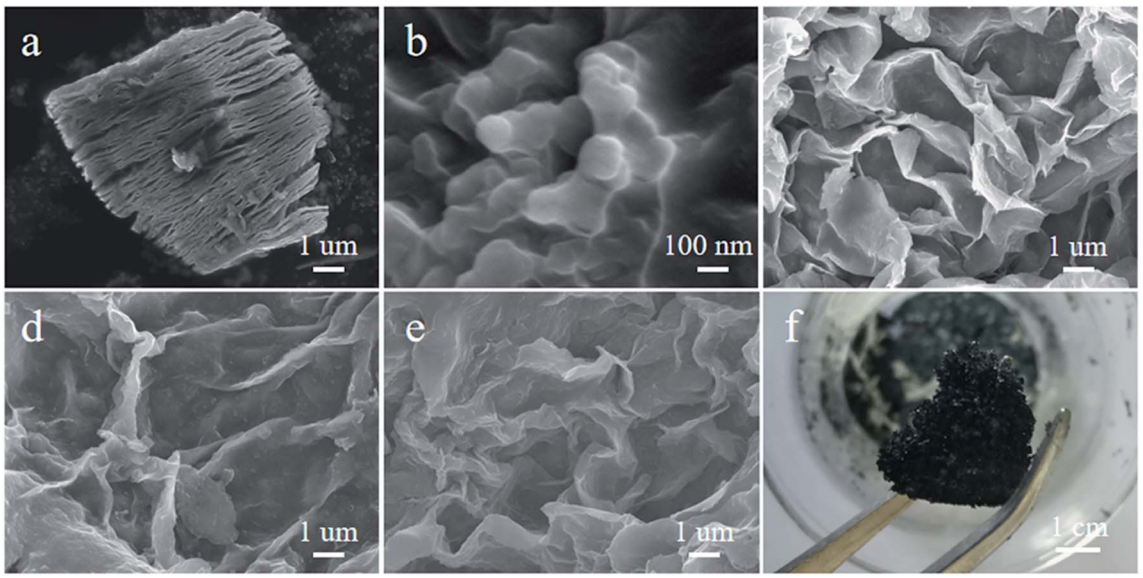

Fig. 2 Morphological characterization of HCl + LiF prepared and the induced $Ti_3C_2T_x$. SEM images of the as-prepared $Ti_3C_2T_x$ (a) HCl + LiF prepared $Ti_3C_2T_x$, (b) monolayer $Ti_3C_2T_x$, (c) alkali-induced $Ti_3C_2T_x$, (d) Co^{2+} induced $Ti_3C_2T_x$, (e) Cd^{2+} induced $Ti_3C_2T_x$, (f) macro morphology of alkali-induced $Ti_3C_2T_x$.

Table 1 Surface area of nitrogen adsorption and desorption of all prepared and induced $Ti_3C_2T_x$

Samples	BET surface area ($m^2\ g^{-1}$)	Langmuir surface area ($m^2\ g^{-1}$)
$Ti_3C_2T_x$–HCl	1.64	2.19
$Ti_3C_2T_x$–HCl–OH	1.79	2.47
$Ti_3C_2T_x$–HCl–Cd	6.50	8.80
$Ti_3C_2T_x$–HCl–Co	16.43	22.49
$Ti_3C_2T_x$–HF	4.61	6.24
$Ti_3C_2T_x$–HF–OH	5.56	7.76
$Ti_3C_2T_x$–HF–Cd	6.87	9.45
$Ti_3C_2T_x$–HF–Co	8.27	11.40

indicates the stabilization of $Ti_3C_2T_x$. The (002) peak analysis shows that ion induction can change the *c*-lattice parameter to a certain extent. For the HCl–LiF-prepared $Ti_3C_2T_x$ (Fig. 3b), the intermediate layer spacing increased visibly which varied from 9.2593 Å of Ti_3AlC_2 to 13.6425 Å for $Ti_3C_2T_x$, while which of alkali-induced and ion-induced are changed slightly compared with $Ti_3C_2T_x$. While the interplanar crystal spacing increases slightly of the HF-etched products (Fig. S4†), and obviously increases from Ti_3AlC_2 9.2593 Å to 12.1438 Å in alkali-induced $Ti_3C_2T_x$, while the tiny variation occurs on Co^{2+} and Cd^{2+} induced multilayer $Ti_3C_2T_x$. The variation in the *c*-lattice parameter which negatively correlates with the variation in layer spacing is also closely related to its performance.

It can be seen in the full XPS spectrum peaks (Fig. S5†) that there is a small Cd peak of both HF-etched $Ti_3C_2T_x$ and HCl–LiF-prepared $Ti_3C_2T_x$ after the induction of Cd^{2+}. The doping of Cd^{2+} may reduce the number of active sites on the $Ti_3C_2T_x$ surface, thus affecting its electrochemical performance. This can be reflected in the CV curve and the charging–discharging performance in the electrochemical test. As shown in C 1s spectra, four peaks at 282.0, 284.6, 285.1 and 288.6 eV were corresponded to C–Ti, C–C, CH_x & C–O, and C–O–O, respectively.[22,23] By observing the C 1s energy spectrum (Fig. 3c and S6†) of different samples, it is manifest that the spectral changes are not obvious, indicating that ion induction has little effect on C 1s.

Both the $2p_{1/2}$ and the $2p_{3/2}$ spin–orbit split components of the Ti 2p spectrum (Fig. 3d and S5†) could be divided into six curves at 454.6 (460.7), 455.3 (461.1), 456.4 (462.1), 458 (463.4), 459 (464.6) and 460 (466.3) eV which were marked as Ti–C, Ti (II), Ti (III), TiO_2, $TiO_{2-x}F_x$ and C–Ti–F_x, respectively.[24–26] Ti–C is in the core of layers whose intensity is associated with *d*-spacing. Thus, the weakening of Ti–C foreshadowed that the exfoliation of Al layers and the greater *d*-spacing of the HCl–LiF-prepared $Ti_3C_2T_x$. $TiO_{2-x}F_x$ and C–Ti–F_x correspond to the surface terminal groups. The percentages of the peak areas of both $TiO_{2-x}F_x$ and C–Ti–F_x are changed visibly after alkali induction and metal ion induction of $Ti_3C_2T_x$. For HCl–LiF-prepared $Ti_3C_2T_x$, the share of the peak field of C–Ti–F_x drops down to 1.12% of alkalized $Ti_3C_2T_x$, 2.48% of Co^{2+} induced $Ti_3C_2T_x$, and 2.99% of Cd^{2+} induced $Ti_3C_2T_x$ from 5.73% of primary $Ti_3C_2T_x$ (Table S1†). Whereas, the proportion of the peak area of $TiO_{2-x}F_x$ of induced $Ti_3C_2T_x$ is upward. For monolayer $Ti_3C_2T_x$, the proportion goes up obviously after alkalization and metal ion induced. Simultaneously, multilayer $Ti_3C_2T_x$ has similar rulers (Table S2 and Fig. S6†). The changes of terminal oxygen–fluorine ratio reveal that the –F surface terminals decrease and the –O surface terminals increase.

3.3. Electrochemical properties of the samples

Fig. 4a and e show the EIS data and equivalent circuit (inserted in Fig. 4a), of the samples, the intermediate frequency curve

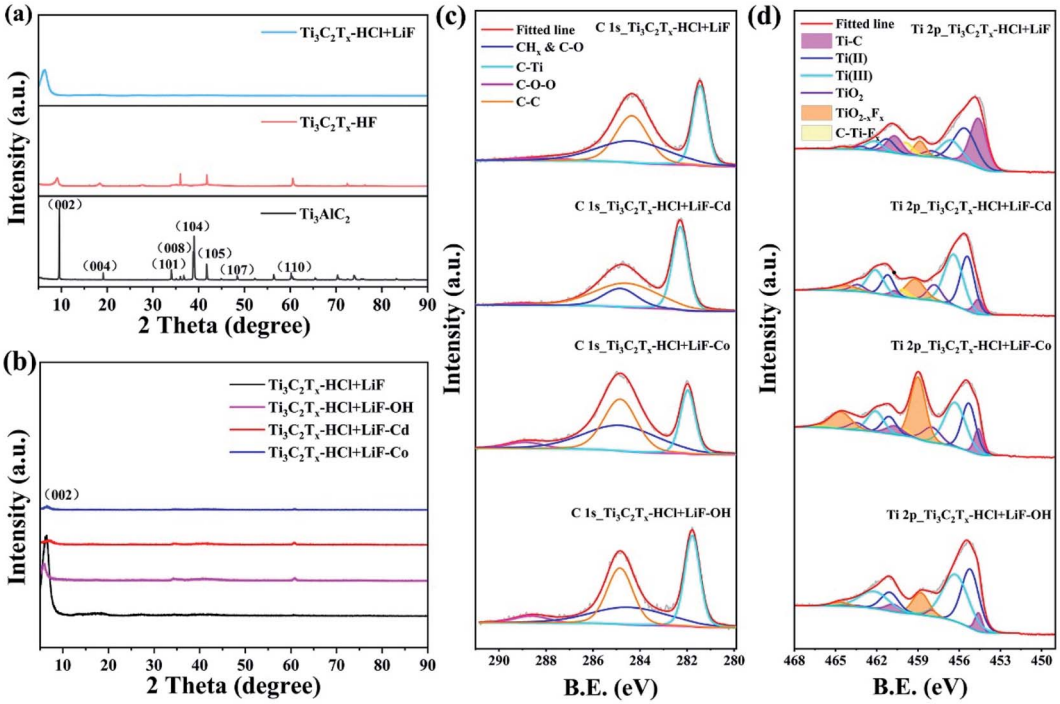

Fig. 3 Structural analysis of HCl + LiF prepared and the induced $Ti_3C_2T_x$. XRD patterns of the as-prepared $Ti_3C_2T_x$ (a) two methods prepared $Ti_3C_2T_x$, (b) induced monolayer $Ti_3C_2T_x$, (c) C 1s XPS spectrum of HCl + LiF prepared $Ti_3C_2T_x$ and induced $Ti_3C_2T_x$, (d) Ti 2p XPS spectrum of HCl + LiF prepared $Ti_3C_2T_x$ and induced $Ti_3C_2T_x$.

with the semicircle represents the charge transfer resistance (R_{ct}) between the electrolyte and the electrode.[14] By comparing the curvature radius, it is clear that alkali-induced MXenes has smaller semicircle diameters, manifesting the faster charge transfer. The lower charge transfer resistance further proves that alkali-induced can supply more electronic pathways and

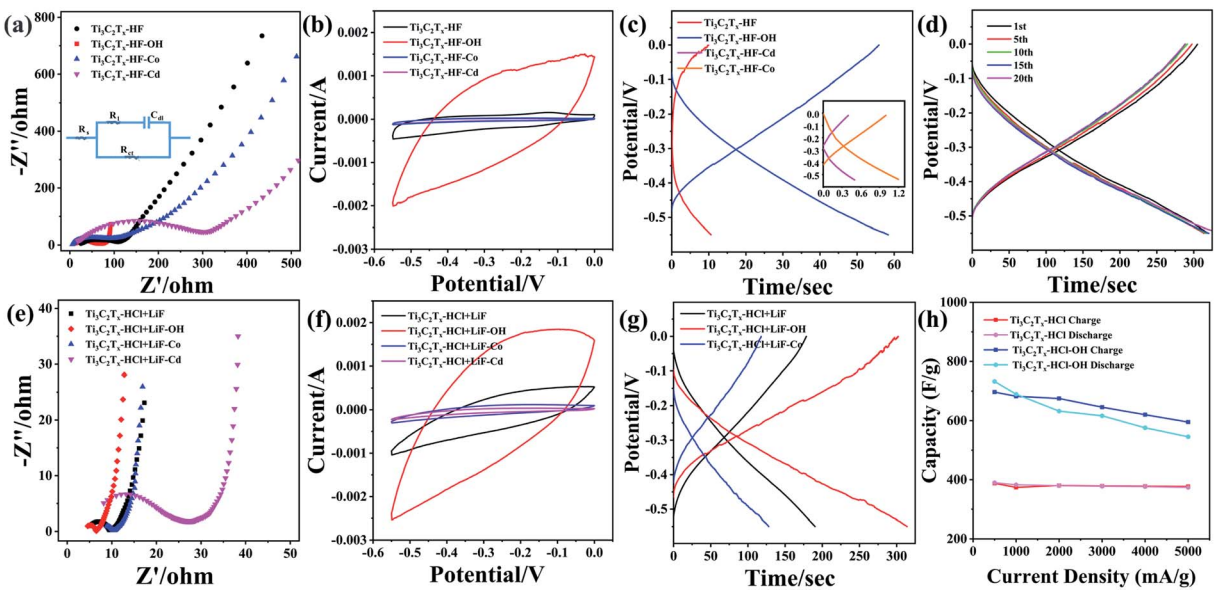

Fig. 4 Electrochemical performance of all as-prepared $Ti_3C_2T_x$. (a) EIS curves of HF prepared and induced $Ti_3C_2T_x$, (b) CV curves of HF prepared and induced $Ti_3C_2T_x$ at −0.55 V to 0 V, (c) discharge–charge profiles of the electrode at a current density of 1 A g^{-1}, (d) cycling stability of the alkali-induced monolayer $Ti_3C_2T_x$, (e) EIS curves of HCl + LiF prepared and induced $Ti_3C_2T_x$, (f) CV curves of HCl + LiF prepared and induced $Ti_3C_2T_x$ at −0.55 V to 0 V, (g) discharge–charge profiles of the electrode at a current density of 1 A g^{-1}, (h) rate performance of HCl + LiF prepared and alkali induced $Ti_3C_2T_x$.

elevate charge transfer kinetics. The low frequency display is determined by diffusion control, which related to the solution resistance (R_s) deeply, and influenced by the layer spacing. The more steep of the slope line, the more surface capacitance reactions are foreboded, and the smaller solution resistance is, which means the better electrochemical performance.[27] Based on the slope of the low-frequency curve, the faster ions diffusion occurred on the alkali-induced MXenes system. However, metal ions induced MXenes have higher electrochemical impedance and concomitantly worse capacitive properties. This conclusion can also be seen in the CV curve (Fig. 4b and f).

As we can see in Fig. S7,† we choose a 10 mV s^{-1} as the scan rate and choose −0.55 V to 0 V as the voltage of the CV and discharge–charge curves. Fig. 4c and g show the discharge–charge profiles of the electrode. According to the charge–discharge curve and $C = It/mV$, the capacitance of $Ti_3C_2T_x$–HF is 32.09 F g^{-1} and $Ti_3C_2T_x$–HF–OH is 124.61 F g^{-1}. The capacitance of HCl–LiF-prepared monolayer $Ti_3C_2T_x$ was 382.67 F g^{-1}, and what of alkali-induced monolayer $Ti_3C_2T_x$ reached 684.53 F g^{-1}. This shows that the electrochemical performance could be greatly improved under alkali induction and electrochemical properties of monolayer $Ti_3C_2T_x$ is more excellent than multilayer $Ti_3C_2T_x$. It is important to point out that the capacitance of the Co^{2+} and Cd^{2+} induced multilayer $Ti_3C_2T_x$ is approximately 2 F g^{-1}, which proves that ion doping has a negative influence on its electrochemical performance due to the oxidation of high-valent metal ions potentially.[19] The capacitance of Co^{2+}-induced monolayer $Ti_3C_2T_x$ is 316.11 F g^{-1}, which is slightly lower than that before induction. When induced by Cd^{2+}, the capacitance performance decreases sharply to about 2 F g^{-1} due to a small amount of ion doping.

Fig. 4d shows the cycling stability of the alkali-induced monolayer $Ti_3C_2T_x$ by discharge/charge curves in the voltage range of −0.55 to 0 V, at a current density of 1 A g^{-1}. The discharge capacity of alkali-induced monolayer MXenes is 684.53 F g^{-1} in the first cycle. Notedly, there were no obvious changes about the capacitance in the fifth and later cycles. Better reproducibility means good reversibility of the electrode. No plateau region signifies that capacitors are most likely the charging mechanism.[28] As shown in Fig. 4h, HCl–$Ti_3C_2T_x$ has better charge and discharge reversibility and rate performance. The discharge capacity of HCl–$Ti_3C_2T_x$ changes from 382.67 F g^{-1} to 373.92 F g^{-1} at a 1000 mA g^{-1} and 5000 mA g^{-1} current density. Apparently, the discharge capacity of the alkali-induced monolayer $Ti_3C_2T_x$ changes from 684.53 F g^{-1} to 545.48 F g^{-1} at a 1000 mA g^{-1} and 5000 mA g^{-1} current density. We put this down to the more chemically active oxygen-containing groups on the surface of alkali-induced monolayer $Ti_3C_2T_x$. More reactive groups potentially mean more side reactions potentially, such as oxidation of MXenes.

Combined with various component and performance analyses, metal ions induced can improve the surface area to some extent, but this does not imply an improvement in electrochemical performance. We can infer that the BET surface area has no direct effect on the capacities. As I mentioned earlier, the –OH surface group has greater electrochemical activity than –F, and alkali induction and metal ions induction can increase the content of –OH surface group in some degree which means a higher capacitance. With largest BET surface area and larger content of –OH surface groups, metal ion-induced $Ti_3C_2T_x$ has a worst capacitance performance. We speculate that the electrochemical performance is not strongly related to the BET surface area for metal ion-induced MXenes. The main reason is that metal ions have a small oxidation ability and can oxidize MXenes.[19] Thus, the capacitance of metal ions induced MXenes decreased instead of growing up, and the alkali-induced MXenes had a better capacity performance.

4. Conclusions

In general, organ-like $Ti_3C_2T_x$, single-deck $Ti_3C_2T_x$ and their revulsive $Ti_3C_2T_x$ were studied to measure electrochemical performance. It is worthwhile to note that the pseudocapacitive performance of HCl–LiF-prepared monolayer $Ti_3C_2T_x$ is better than organ-like $Ti_3C_2T_x$ of HF-etched. Compared with $Ti_3C_2T_x$, an excellent capacitance of 684.53 F g^{-1} could be obtained for the alkalized single-deck $Ti_3C_2T_x$. The abduction of metal ions has some negative effects on electrochemical properties because of the oxidation of high-valent metal ions. However, whether the alkali-induced or metal ion induced methods can let –O terminal groups replace –F terminal groups completely, which means that the electrochemical performance can be further improved. Improving the electrochemical activity of metal ions induced MXenes with a higher surface area is a problem demanding prompt solution. There is shortened lifetime and poor rate performance due to factors such like oxidation and chemical activity. Those questions deserve further inquiry.

Conflicts of interest

The authors declare that they have no known competing financial interests or personal relationships that could have appeared to influence the work reported in this paper.

Acknowledgements

This work was supported by the National Natural Science Foundation of China (51775532), the project ZR2020ZD29 and ZR2021JQ20 supported by Shandong Provincial Natural Science Foundation, the Taishan Scholars Program of Shandong Province.

References

1 M. Boota, B. Anasori, C. Voigt, M. Q. Zhao, M. W. Barsoum and Y. Gogotsi, Pseudocapacitive Electrodes Produced by Oxidant-Free Polymerization of Pyrrole between the Layers of 2D Titanium Carbide (MXene), *Adv. Mater.*, 2016, **28**(7), 1517–1522.

2 X. Wang, S. Kajiyama, H. Iinuma, E. Hosono, S. Oro, I. Moriguchi, M. Okubo and A. Yamada, Pseudocapacitance of MXene nanosheets for high-power sodium-ion hybrid capacitors, *Nat. Commun.*, 2015, **6**, 6544.

3 Z. Ling, C. E. Ren, M. Q. Zhao, J. Yang, J. M. Giammarco, J. Qiu, M. W. Barsoum and Y. Gogotsi, Flexible and conductive MXene films and nanocomposites with high capacitance, *Proc. Natl. Acad. Sci. U. S. A.*, 2014, **111**(47), 16676–16681.

4 M. Ghidiu, M. R. Lukatskaya, M. Q. Zhao, Y. Gogotsi and M. W. Barsoum, Conductive two-dimensional titanium carbide clay with high volumetric capacitance, *Nature*, 2014, **516**(7529), 78–81.

5 J. Li, X. Yuan, C. Lin, Y. Yang, L. Xu, X. Du, J. Xie, J. Lin and J. Sun, Achieving High Pseudocapacitance of 2D Titanium Carbide (MXene) by Cation Intercalation and Surface Modification, *Adv. Energy Mater.*, 2017, **7**(15), 1602725.

6 W. M. Barsoum and T. El-Raghy, The MAX phases: Unique new carbide and nitride materials – Ternary ceramics turn out to be surprisingly soft and machinable, yet also heat-tolerant, strong and lightweight, *Am. Sci.*, 2001, **89**(4), 334–343.

7 B. Anasori, Y. Xie, M. Beidaghi, J. Lu, B. C. Hosler, L. Hultman, P. R. C. Kent, Y. Gogotsi and M. W. Barsoum, Two-Dimensional, Ordered, Double Transition Metals Carbides(MXenes), *ACS Nano*, 2015, **9**, 9507–9516.

8 M. Alhabeb, K. Maleski, B. Anasori, P. Lelyukh, L. Clark, S. Sin and Y. Gogotsi, Guidelines for Synthesis and Processing of Two-Dimensional Titanium Carbide ($Ti_3C_2T_x$ MXene), *Chem. Mater.*, 2017, **29**(18), 7633–7644.

9 B. Anasori, M. R. Luhatskaya and Y. Gogotsi, 2D Metal carbides and nitrides (MXenes) for energy storage, *Nat. Rev. Mater.*, 2017, **2**(10), 16098.

10 Q. Tao, M. Dahlqvist, J. Lu, S. Kota, R. Meshkian, J. Halim, J. Palisaitis, L. Hultman, M. W. Barsoum, P. O. A. Persson and J. Rosen, Two-dimensional Mo1.33C MXene with divacancy ordering prepared from parent 3D laminate with in-plane chemical ordering, *Nat. Commun.*, 2017, **8**, 14949.

11 J. Zhou, X. Zha, X. Zhou, F. Chen, G. Gao, S. Wang, C. Shen, T. Chen, C. Zhi, P. Eklund, S. Du, J. Xue, W. Shi, Z. Chai and Q. Huang, Synthesis and Electrochemical Properties of Two-Dimensional Hafnium Carbide, *ACS Nano*, 2017, **11**(4), 3841–3850.

12 Y. Dall'Agnese, M. R. Lukatskaya, K. M. Cook, P. L. Taberna, Y. Gogotsi and P. Simon, High capacitance of surface-modified 2D titanium carbide in acidic electrolyte, *Electrochem. Commun.*, 2014, **48**, 118–122.

13 M. Naguib, V. N. Mochalin, M. W. Barsoum and Y. Gogotsi, 25th Anniversary article: MXenes: a new family of two-dimensional materials, *Adv. Mater.*, 2014, **26**(7), 992–1005.

14 X. Wang, J. Wang, J. Qin, X. Xie, R. Yang and M. Cao, Surface Charge Engineering for Covalently Assembling Three-Dimensional MXene Network for All-Climate Sodium Ion Batteries, *ACS Appl. Mater. Interfaces*, 2020, **12**(35), 39181–39194.

15 M. R. Lukatskaya, O. Mashtalir, C. E. Ren, Y. Dall'Agnese, P. Rozier, P. L. Taberna, M. Naguib, P. Simon, M. W. Barsoum and Y. Gogotsi, Cation intercalation and high volumetric capacitance of two-dimensional titanium carbide, *Science*, 2013, **341**(6153), 1502–1505.

16 O. Mashtalir, M. Naguib, V. N. Mochalin, Y. Dall'Agnese, M. Heon, M. W. Barsoum and Y. Gogotsi, Intercalation and delamination of layered carbides and carbonitrides, *Nat. Commun.*, 2013, **4**, 1716.

17 D. Zhao, M. Clites, G. Ying, S. Kota, J. Wang, V. Natu, X. Wang, E. Pomerantseva, M. Cao and M. W. Barsoum, Alkali-induced crumpling of $Ti_3C_2T_x$ (MXene) to form 3D porous networks for sodium ion storage, *Chem. Commun.*, 2018, **54**, 4533–4536.

18 D. Zhao, R. Zhao, S. Dong, X. Miao, Z. Zhang, C. Wang and L. Yin, Alkali-induced 3D crinkled porous Ti_3C_2 MXene architectures coupled with NiCoP bimetallic phosphide nanoparticles as anodes for high-performance sodium-ion batteries, *Energy Environ. Sci.*, 2019, **12**(8), 2422–2432.

19 Y. Deng, T. Shang, Z. Wu, Y. Tao, C. Luo, J. Liang, D. Han, R. Lyu, C. Qi, W. Lv, F. Kang and Q. H. Yang, Fast Gelation of $Ti_3C_2T_x$ MXene Initiated by Metal Ions, *Adv. Mater.*, 2019, **31**(43), e1902432.

20 M. Naguib, O. Mashtalir, J. Carle, V. Presser, J. Lu, L. Hultman, Y. Gogotsi and M. W. Barsoum, Two-dimensional transition metal carbides, *ACS Nano*, 2012, **6**(2), 1322–1331.

21 Q. Zhang, H. Lai, R. Fan, P. Ji, X. Fu and H. Li, High Concentration of $Ti_3C_2T_x$ MXene in Organic Solvent, *ACS Nano*, 2021, **15**(3), 5249–5262.

22 Z. Yang, A. Liu, C. Wang, F. Liu, J. He, S. Li, J. Wang, R. You, X. Yan, P. Sun, Y. Duan and G. Lu, Improvement of Gas and Humidity Sensing Properties of Organ-like MXene by Alkaline Treatment, *ACS Sens.*, 2019, **4**(5), 1261–1269.

23 X. Chen, Y. Zhu, M. Zhang, J. Sui, W. Peng, Y. Li, G. Zhang, F. Zhang and X. Fan, *N*-Butyllithium-Treated $Ti_3C_2T_x$ MXene with Excellent Pseudocapacitor Performance, *ACS Nano*, 2019, **13**(8), 9449–9456.

24 J. Halim, M. R. Lukatskaya, K. M. Cook, J. Lu, C. R. Smith, L.-Å. Näslund, S. J. May, L. Hultman, Y. Gogotsi, P. Eklund and M. W. Barsoum, Transparent Conductive Two-Dimensional Titanium Carbide Epitaxial Thin Films, *Chem. Mater.*, 2014, **26**(7), 2374–2381.

25 M. Benchakar, L. Loupias, C. Garnero, T. Bilyk, C. Morais, C. Canaff, N. Guignard, S. Morisset, H. Pazniak, S. Hurand, P. Chartier, J. Pacaud, V. Mauchamp, M. W. Barsoum, A. Habrioux and S. Célérier, One MAX phase, different MXenes: A guideline to understand the crucial role of etching conditions on $Ti_3C_2T_x$ surface chemistry, *Appl. Surf. Sci.*, 2020, **530**, 147209.

26 J. Halim, K. M. Cook, M. Naguib, P. Eklund, Y. Gogotsi, J. Rosen and M. W. Barsoum, X-ray photoelectron spectroscopy of select multi-layered transition metal carbides (MXenes), *Appl. Surf. Sci.*, 2016, **362**, 406–417.

27 C. Ding, F. Dong and Z. Tang, Construction of hollow carbon polyhedron supported Pt catalyst for methanol electrocatalytic oxidation, *Electrochim. Acta*, 2021, **390**, 138790.

28 Y. Dall'Agnese, P. L. Taberna, Y. Gogotsi and P. Simon, Two-Dimensional vanadium carbide (MXene) as positive electrode for sodium-ion capacitors, *J. Phys. Chem. Lett.*, 2015, **6**, 2305–2309.